Universidade de Coimbra

Faculdade de Ciências e Tecnologia

Departamento de Física

Electronic Properties of Doped Silicon Nanocrystals

Estelina Lora da Silva

2010

Universidade de Coimbra

Faculdade de Ciências e Tecnologia

Departamento de Física

Electronic Properties of Doped Silicon Nanocrystals

Dissertação submetida à Faculdade de Ciências e Tecnologia da Universidade de Coimbra para apreciação em provas do Curso de Mestrado em Física, com especialização em Modelação e Simulação Computacional

Orientação:

Prof. Doutor Fernando Nogueira
Universidade de Coimbra

Doutor José Pedro Coutinho
Universidade de Aveiro

Estelina Lora da Silva

2010

Acknowledgments

I would like to thank my supervisors, Profs. José Coutinho and Fernando Nogueira, for allowing all the necessary conditions required in the elaboration of the present work and for always willing to help, without hesitation and promptly, when suggestions and indications were needed.

I also wish to extend my gratitude to the members of the Centre for Computational Physics, the Condensed Matter research unit, Apostolos Marinopoulos, Bruce Forbes, Claudia Cardoso, Duan-Juan Cai, José Rui de Sousa, Myrta Grüning, Micael Oliveira, Paulo de Abreu and Rui Travasso, for all the helpful discussions and incites in the resolution of some problems that emerged during the calculations.

Abstract

A density functional modelling study of impurities in hydrogen terminated silicon nanocrystals is presented. Energy states of some contenders for n- and p-type doping in confined systems are calculated, namely for the first three interstitial alkali elements, Li, Na and K, and the first three interstitial halogen elements, F, Cl and Br. We find that these impurities do not contribute with carriers (electrons or holes) to the LUMO or HOMO states at room temperature. This results from both surface confinement and electronic weak screening in the nanocrystals. Energy levels for P, B and the O_5 chain model for the Thermal Double Donors (TDD) were also calculated in order to assess their behaviour in the confined systems *vs* the well established dopant character bulk. Deep energy levels were also found for these impurities.

Resumo

No presente trabalho estuda-se, através de modelação computacional baseada na teoria do funcional da densidade, os efeitos de impurezas em nanocristais de silício passivados com hidrogénio. São calculados os níveis de energia das impurezas intersticiais mais propícias à dopagem de tipo-n e p para os sistemas confinados, nomeadamente os três primeiros elementos pertencentes ao grupo dos alcalinos, Li, Na e K, e os três primeiros halogéneos, F, Cl e Br. Observou-se que à temperatura ambiente estas impurezas não contribuem com portadores de carga (electrões ou lacunas) para os estados HOMO nem LUMO. Este facto resulta do confinamento da superfície e do meio dieléctrico fraco existente no nanocristal. Os níveis de energia para o P, B e o Duplo Dador Térmico do modelo da cadeia O_5 foram também calculados por forma a comparar o comportamento destes nos sistemas confinados com o comportamento, bem estabelecido, na matéria extensa. Níveis de energia profundos no hiato também foram observados para estas impurezas.

Contents

List of Tables

List of Figures

Chapter 1

Introduction

Since much attention is being drawn to nano-optoelectronic devices, with promising technological and medical applications (molecular photosensitization, colour-dyes, new generation of solar cell applications, Li-ion batteries), the understanding of the electrical and optical properties of Si nanocrystals (Si-NC) becomes an important aspect to focus upon, due to the fact that these systems possess different properties from those of the bulk materials.

Nanostructures, smaller than macroscopic objects (present-day electronic devices), but larger than molecules, belong to the intermediate domain of a complex combination of classical physics and quantum mechanics, where amazing properties emerge - the mesoscopic world.

Quantum effects become dominant when the nanometre size range is reached, thus accounting for changes in the physical properties of nanostructures, as is the case for the increase in surface area to volume ratio altering mechanical and thermal properties of materials. Here, the geometry of the material can dictate drastic effects on quantized states. The energy spectrum becomes discrete, measured as quanta, rather than continuous as in bulk materials. As a result, the bandgap becomes size dependent and this is known as the quantum confinement effect.

The present report is divided into four chapters. The first, is an overview of the theoretical background and a brief introduction to the relevance of the study of undoped and doped silicon nanocrystals - the enhancement of the surface-area effects that are responsible for the appearance of different properties when compared to those of bulk silicon. The second chapter accounts for the description and convergence parameters defined in the computer codes for the systems under study. The third chapter goes through a discussion

of the obtained results, where in the first section this is based on the evaluation of energy gaps for different sized systems, in order to compare data from relevant literature and also to compare results between two exchange-correlation functionals - LDA and GGA. The second section accounts for the study of energy states of the doped silicon nanocrystals with the aim of fingding possible contenders to act as shallow impurities in silicon nanocrystals. The fourth chapter finalizes the report with the importance and conclusions of the present work and describes future studies of oxidized silicon nanocrystals, where core-shell transfer doping effects may occur, and the evaluation of optical properties of silicon nanocrystals.

1.1 Density Functional Theory

1.1.1 The Many-Body Problem

In order to solve the many body Schrödinger's equation for a quantum system of N interacting fermions, several approximations can be employed, being these simplifications of the full problem of many electrons moving in an external, electrostatic potential field.

In the absence of external fields, the many-body Schrödinger equation, involving a set of N_e electrons and N_n atomic nuclei, is

$$\widehat{H}\Psi(\vec{R},\vec{r}) = E\Psi(\vec{R},\vec{r}), \tag{1.1}$$

where the wavefunction of the system depends on the nuclei, $\vec{R}$, and the electron, $\vec{r}$, positions. This interacting system is usually described by the Hamiltonian, $\widehat{H}$, containing the kinetic and potential terms [1]

$$\widehat{H} = -\frac{1}{2}\sum_{i}^{N_e}\nabla_i^2 - \sum_{\alpha}^{N_n}\frac{1}{2M_\alpha}\nabla_\alpha^2 + \frac{1}{2}\sum_{\substack{i,j=1\\ i\neq j}}^{N_e}\frac{1}{|\vec{r}_i-\vec{r}_j|} - \sum_{i,\alpha=1}^{N_e,N_n}\frac{Z_\alpha}{|\vec{r}_i-\vec{R}_\alpha|} + \frac{1}{2}\sum_{\substack{\alpha,\beta=1\\ \alpha\neq\beta}}^{N_n}\frac{Z_\alpha Z_\beta}{|\vec{R}_\alpha-\vec{R}_\beta|}, \tag{1.2}$$

where M_α, Z_α and $\vec{R}_\alpha$ represent the mass, charge and location of the α-th nucleus, and $\vec{r}_i$ the coordinate of the i-th electron. The total wavefunction is thus a function of N_n plus N_e coordinates (disregarding spin degrees of freedom), respectively [1],

$$\Psi \equiv \Psi(\vec{r}_1,\ldots,\vec{r}_{N_e};\vec{R}_1,\ldots,\vec{R}_{N_n}). \tag{1.3}$$

[1] Quantities are expressed in atomic units, where $\hbar$, electron charge e, electron mass m and permitivity of vacuum $4\pi\epsilon_0$, are taken to be unity.

One of the first simplifications to solve the many-body problem was the Born-Oppenheimer approximation (1927). This approach considered that the Schrödinger equation, for the electronic system, could be solved in a field of static nuclei, due to the mass of the nuclei being ~ 2000 times bigger than the mass of the electrons. Thus, the nuclear and electronic degrees of freedom can be separated, which implies that electrons are supposed to move in a potential of nuclei frozen in their equilibrium positions (adiabatic approximation).

The total wavefunction can then be approximated as

$$\Psi(\vec{r},\vec{R}) = \psi(\vec{r},\vec{R})\phi(\vec{R}) \tag{1.4}$$

where ψ and ϕ are separate electronic and nuclear wavefunctions (the electronic wavefunction depends on $\vec{R}$ in a parametric way), and the Born-Oppenheimer Hamiltonian for the electrons reads

$$\widehat{H}_{\mathrm{BO}} = -\frac{1}{2}\sum_{i}^{N_e}\nabla_i^2 + \frac{1}{2}\sum_{\substack{i,j=1\\ i\neq j}}^{N_e}\frac{1}{|\vec{r}_i-\vec{r}_j|} - \sum_{i,\alpha=1}^{N_e,N_n}\frac{Z_\alpha}{|\vec{r}_i-\vec{R}_\alpha|}. \tag{1.5}$$

Even though the positions of the nuclei are kept fixed, finding the electronic wave function remains a difficult task to achieve, because the Coulomb interaction (interactions between electrons), second term of Eq. 1.5, introduces correlations between electrons.

When it is not possible to disregard the connection between electrons and nuclei, such as for systems where electron-phonon coupling is a fundamental parameter (Jahn-Teller systems, superconductor materials) [1], this approach cannot be applied.

Hartree (1928) attempted to replace the Coulomb interaction by an effective electron-electron potential, $U_{\mathrm{ee}}(\vec{r})$, in which each electron moves in a field produced by a sum over all the other electrons. This term was suggested to be of the form

$$U_{\mathrm{ee}}(\vec{r}) = \int d\vec{r}'\frac{n(\vec{r}')}{|\vec{r}-\vec{r}'|}, \tag{1.6}$$

with n being the density of electrons

$$n(\vec{r}) = \sum_j |\psi_j(\vec{r})|^2. \tag{1.7}$$

In this simple approximation, electronic correlation is not accounted for and the many-body Schrödinger equation is decoupled into N_e one-electron equations. This results in

the Hartree equation [2]

$$-\frac{1}{2}\nabla^2\psi_l + [U_{\text{ion}}(\vec{r}) + U_{\text{ee}}(\vec{r})]\psi_l = \varepsilon_l\psi_l \tag{1.8}$$

where U_{ion} is the ion interaction potential.

Due to the nature of the Hartree equation, Eq. 1.8 (one-electron equation), the Pauli principle is not recognized - whenever two electrons occupy the same position, the true many-body wavefunction has to vanish. Fock and Slater (1930) suggested that due to the fermionic character of the electrons, a space of antisymmetric wavefunctions is required, where the many-electron wavefunction has the form of an antisymmetrised product of one-electron wavefunctions [3, 2].

The simplest possible type of antisymmetric wavefunction is obtained by taking a collection of orthonormal one-particle wavefunctions

$$\int \psi_i^*(\vec{r})\psi_j(\vec{r})d\vec{r} = \delta_{ij} \tag{1.9}$$

and antisymmetrizing them, in the form of a Slater determinant

$$\Psi(\vec{r}_1\sigma_1\cdots\vec{r}_N\sigma_N) = \frac{1}{\sqrt{N!}}\sum_s (-1)^s \psi_{s_1}(\vec{r}_1\sigma_1)\cdots\psi_{s_N}(\vec{r}_N\sigma_N) \tag{1.10}$$

$$= \frac{1}{\sqrt{N!}}\begin{vmatrix} \psi_1(\vec{r}_1\sigma_1) & \psi_1(\vec{r}_2\sigma_2) & \cdots & \psi_1(\vec{r}_N\sigma_N) \\ \vdots & \vdots & \ddots & \vdots \\ \psi_n(\vec{r}_1\sigma_1) & \psi_n(\vec{r}_2\sigma_2) & \cdots & \psi_n(\vec{r}_N\sigma_N) \end{vmatrix} \tag{1.11}$$

where the sum is over all permutations s (the sign is $+1$ or -1 whether the permutation can be written as a product of an even or odd number of pair interchanges).

Because this wavefunction is not a simple product, but a determinant, the Pauli principle induces correlations among particles and therefore, the spin index σ_i (taking values ± 1) is included in every wavefunction. The wavefunction can be written in the form

$$\psi_l(\vec{r}_i\sigma_i) = \psi_l(\vec{r}_i)\chi_l(\sigma_i) \tag{1.12}$$

being $\chi_l(\sigma_i)$ the spin-function, satisfying [4]

$$\sum \chi_l^*(\sigma_i)\chi_k(\sigma_i) = \delta_{lk}. \tag{1.13}$$

The expectation value of the energy, is

$$E = \sum_l \langle \psi_l | h_l + \frac{1}{2}(J_l - K_l) | \psi_l \rangle, \tag{1.14}$$

where $\hat{h} = \sum_l h_l$ is the one-electron integral of the form

$$h_l = \frac{1}{2}\nabla_l^2 - \sum_n \frac{Z_n}{\vec{r}_l - \vec{R}_n}, \tag{1.15}$$

$\hat{J} = \sum_l J_l$ is the Coulomb operator (electron-electron repulsion term) and $\hat{K} = \sum_l K_l$ the exchange operator (spin-correlation effects), with

$$J_l(\vec{r}) = \sum_k \int\int \psi_l(\vec{r})\psi_l^*(\vec{r})\frac{1}{|\vec{r} - \vec{r'}|}\psi_k(\vec{r'})\psi_k^*(\vec{r'})\, d\vec{r}\, d\vec{r'} \tag{1.16}$$

$$K_l(\vec{r}) = \sum_k \int\int \psi_l(\vec{r})\psi_k^*(\vec{r})\frac{1}{|\vec{r} - \vec{r'}|}\psi_k(\vec{r'})\psi_l^*(\vec{r'})\, d\vec{r}\, d\vec{r'}. \tag{1.17}$$

By minimizing 1.14 as a function of the spin-orbitals, ψ_l, providing the many-electron ground-state, this gives the Hartree-Fock equations

$$\hat{F}\psi_l = \epsilon_l \psi_l, \tag{1.18}$$

where $\hat{F}$ is known as the Fock operator (effective one-electron operator), defined as $\hat{F} = \hat{h} + \hat{J} - \hat{K}$.

Equation 1.18 is a Schrödinger-like equation, with ϵ_l being a lagrange multiplier, that have to be chosen such it ensures orbital orthonormalization, and is identified as the orbital energies.

Density Function Theory (DFT) is based on the work performed on electronic structure calculations for solids by Hohenberg, Kohn and Sham in 1965 [5, 6]. Here the electronic orbitals are solutions of a set of Schrödinger-like equations (referred to as Kohn-Sham equations), from which potential terms depend on the electron density rather than on the individual electron orbitals, as in the Hartree-Fock theory.

In Hartree-Fock the potential terms enter the equations in a non-local way - the value of the Coulomb and the exchange operators at $\vec{r}$ depends on the coordinate $\vec{r'}$, complicating

the evaluation of their respective matrix elements [1]. Within DFT, the Hamiltonian has a non-local dependence on the density, however this value can be taken to depend on the local value of the density alone with approximations made to the exchange-correlation potential, simplifying the evaluation of the Kohn-Sham solutions.

Since the electron density, $n(\vec{r})$, is a simple function that depends solely on the 3-dimensional vector $\vec{r}$, instead of the $3N$ coordinates of the many-body wavefunction, where N is the number of electrons of the system, the density is used as basic variable and thus density functional theory becomes computationally feasible for large systems [7].

This theory is the theoretical foundation for the construction of an effective single-particle scheme allowing for the accurate calculation of the ground state density and energy of systems of interacting electrons [7].

The Kohn-Sham method assumes that, for each interacting ground state density $n(\vec{r})$, there is a non-interacting electron system with the same ground state density. The interacting ground state is thus obtained through the solution of the Kohn-Sham equations that have the form of the single-particle Schrödinger equation

$$\Big[-\frac{\nabla^2}{2} + v_{\mathrm{KS}}[n(\vec{r})]\Big]\varphi_i(\vec{r}) = \epsilon_i\varphi_i(\vec{r}),$$

where v_{KS} is the Kohn-Sham potential, with a functional dependence on the electronic density, n, which is defined in terms of the Kohn-Sham wave-functions by

$$n(\vec{r}) = \sum_{i}^{occ} |\varphi_i(\vec{r})|^2.$$

This potential can be defined as the sum of the external potential, the Hartree term and the exchange and correlation potential (xc), thus

$$v_{\mathrm{KS}}[n(\vec{r})] = v_{\mathrm{ext}}(\vec{r}) + v_{\mathrm{Hartree}}[n(\vec{r})] + v_{\mathrm{xc}}[n(\vec{r})]. \tag{1.19}$$

Each component of Eq. 1.19 is solved according to the following:

1. The external potential is a sum of nuclear potentials centered at the atomic positions

$$v_{\mathrm{ext}}(\vec{r}) \;=\; \sum_{\alpha} v_{\alpha}(\vec{r} - \vec{R}_{\alpha}) \tag{1.20}$$

This term is the Coulomb attraction between the bare nucleus and the electrons $v_\alpha = -Z_\alpha/r$ (with Z_α being the nuclear charge), but, when necessary, this potential can be replaced by Pseudopotentials, an effective interaction between the valence electrons and an ionic core consisting of the nucleus and the inner electrons (detailed discussion in subsection 1.1.2).

2. The Hartree term (electrostatic energy of the electron in the field generated by the total density) can be evaluated by direct integration

$$v_{\text{Hartree}}[n(\vec{r})] = \int d^3r' \frac{n(\vec{r'})}{|\vec{r} - \vec{r'}|} \tag{1.21}$$

or by solving the Poisson equation

$$\nabla^2 v_{\text{Hartree}}[n(\vec{r})] = -4\pi[n(\vec{r})]$$

3. The xc potential takes into account the many-body effects in the form of an exchange-correlation functional and is defined by the functional derivative of the xc energy (discussed in subsection 1.1.3)

$$v_{\text{xc}}[n(\vec{r})] = \frac{\delta E_{\text{xc}}}{\delta n(\vec{r})}. \tag{1.22}$$

1.1.2 Pseudopotentials

The chemical binding of atoms is due almost exclusively to the valence electrons. The inner core electrons can thus be disregarded, forming an inert core, with the nucleus, that interacts with the valence electrons [8].

The concept of pseudopotential was first proposed by Fermi in 1934 [9] and in 1935, Hellman [10], suggested for potassium, that the potential felt by the valence electron could be represented by

$$w(\vec{r}) = -\frac{1}{r} + \frac{2.74}{r} e^{-1.16r},$$

thus replacing the complicated effects from core electrons by using an effective potential (pseudopotential). Based on this idea, the Schrödinger equation will now contain a modified effective potential term instead of an explicit Coulombic potential for core electrons.

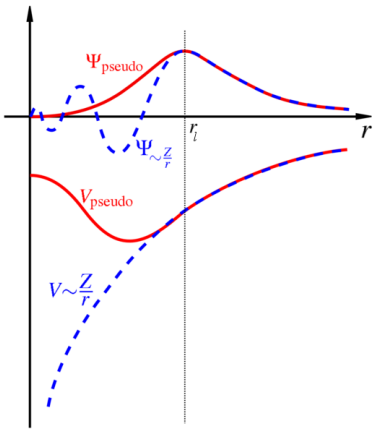

Figure 1.1: Comparison of a wavefunction in the Coulomb potential of the nucleus (blue) to the one in the pseudopotential (red). The real and the pseudowavefunction and potentials match above a certain cut-off radius r_l.

The wavefunction can be written as a sum of a smooth function (pseudowavefunction) with an oscillating wavefunction resulting from the orthogonalization between the valence and the core electrons [8]

$$|\psi_v\rangle = |\varphi_v\rangle + \sum_c \alpha_{cv}|\psi_c\rangle, \tag{1.23}$$

where $\alpha_{cv} = -\langle\psi_c|\varphi_v\rangle$, $|\psi_v\rangle$ and $|\psi_c\rangle$ are the exact solutions of the Schrödinger equation for the valence and the core electrons, respectively, and $|\varphi_v\rangle$ the pseudowavefunction. This avoids the violation of the Pauli exclusion principle since orthogonality ensures that core electrons do not occupy filled valence orbitals.

The Schrödinger equation for the smooth orbital $|\varphi_v\rangle$ is thus

$$\widehat{H}|\varphi_v\rangle = E_v|\varphi_v\rangle + \sum_c (E_c - E_v)|\psi_c\rangle\langle\psi_c|\varphi_v\rangle. \tag{1.24}$$

Nowadays there are two main types of pseudopotentials in use: norm-conserving and ultrasoft pseudopotentials.

Norm-conserving pseudopotentials are constructed by using an *ab-initio* procedure and require that the pseudo- and all-electron valence eigenstates have the same energies, amplitude, and charge densities outside a certain cut-off radius, r_l - fig. 1.1. The integrated charge inside the cut-off radius for each wavefunction must agree (norm-conservation), so that the total charge in the core region is correct and that the normalized pseudo-orbital

equals the true orbital outside r_l [11], therfore requiring that the pseudo wavefunction has the same norm as the true valence wavefunctions [8]. The norm-conserving condition is defined as

$$R_l^{\mathrm{PP}}(\vec{r}) = R_{nl}^{\mathrm{AE}}(\vec{r}), \qquad \text{if } r > r_l \tag{1.25}$$

$$\int_0^{r_l} dr |R_l^{\mathrm{PP}}(\vec{r})|^2 \, r^2 = \int_0^{r_l} dr |R_{nl}^{\mathrm{AE}}(\vec{r})|^2 \, r^2, \qquad \text{if } r < r_l \tag{1.26}$$

where $R_l(\vec{r})$ is the radial part of the wavefunction with angular momentum l, and PP and AE are the pseudo and the all-electron wavefunction, respectively.

The cut-off radius can influence the accuracy to reproduce the realistic features in different environments (transferability), being r_l the measure of the quality of the pseudopotential. The minimum value for the cut-off radius is determined by the location of the outermost nodal surface of the true wavefunction, to remove the oscillations in the core region - if r_l is close to this minimum, the pseudopotential can reproduce the system more accurately (strong pseudopotential). If a very large cut-off radius is chosen, the pseudopotential will be smooth and almost angular momentum independent (softer pseudopotential), not being adequate to transfer between widely varying systems. A soft potential leads to a fast convergence of plane wave basis calculations, being the choice of the ideal cut-off radius a *balance* between basis-set size and pseudopotential accuracy. The ultrasoft pseudopotentials, where norm-conservation is not enforced, are constructed to describe a particular atomic environment [8].

1.1.3 Exchange-Correlation Potential

One of the differences between the Hartree-Fock approximation and DFT is the replacement of the exchange term by the exchange correlation energy E_{xc} - functional of the density, including, not only the exchange effects, but also dynamic correlation effects due to the Coulomb repulsion between the electrons [3].

The exchange-correlation potential is a functional derivative of the exchange-correlation energy, Eq. 1.22, with respect to the local density. To ensure that the Kohn-Sham formulation is exact, the xc energy can be defined as

$$E_{\mathrm{xc}}[n(\vec{r})] = T[n(\vec{r})] - T_s[n(\vec{r})] + E_{\mathrm{ee}}[n(\vec{r})] - E_{\mathrm{Hartree}}[n(\vec{r})] \tag{1.27}$$

where $T[n(\vec{r})]$ and $E_{\rm ee}[n(\vec{r})]$ are the exact kinetic and electron-electron interaction energies, respectively, $T_s[n(\vec{r})]$ is the Kohn-Sham kinetic energy

$$T_s[n(\vec{r})] = \sum_{i=1} \int \psi_i^*(\vec{r}) \Big(-\frac{1}{2}\nabla^2 \Big) \psi_i(\vec{r})\, dr \tag{1.28}$$

and $E_{\rm Hartree}$ is the classical Hartree energy of the electrons of the form

$$E_{\rm Hartree}[n(\vec{r})] = \frac{1}{2} \int \int \frac{n(\vec{r}) n(\vec{r}')}{|\vec{r} - \vec{r}'|}\, dr dr'. \tag{1.29}$$

The kinetic and interaction terms can be group into an universal functional, equal to all electron systems and independent of the external potential, as

$$F_{\rm HK}[n(\vec{r})] = T[n(\vec{r})] + E_{\rm ee}[n(\vec{r})], \tag{1.30}$$

where the HK subscript refers to the the Hohenberg-Kohn theory, where this functional is originated from. Thus, the $E_{\rm xc}$ can be written in terms of Hohenberg-Kohn functional as [11]

$$E_{\rm xc}[n(\vec{r})] = F_{\rm HK}[n(\vec{r})] - (T_s[n(\vec{r})] + E_{\rm Hartree}[n(\vec{r})]). \tag{1.31}$$

For a homogeneous electron gas, the potential will depend only on the value of the electron density. For an inhomogeneous system, the value of the exchange-correlation potential at point $\vec{r}$ depends not only on the value of the density at $\vec{r}$, but also on its variation close to $\vec{r}$, and can be therefore written as an expansion in the gradients

$$V_{\rm xc}[n(\vec{r})] = V_{\rm xc}[n(\vec{r}), \nabla n(\vec{r}), \nabla(\nabla n(\vec{r})), \dots]. \tag{1.32}$$

The inclusion of density gradients is not needed in most cases, so the simplest approximation to represent an exchange correlation potential is to apply the Local Density Approximation (LDA) or its spin-relaxed version, the Local Spin-Density Approximation (LSDA) - here the potential depends only on the value of the density at $\vec{r}$ and not on its gradients. The functional has the form [8]

$$E_{\rm xc}^{\rm LDA} = \int d^3r \varepsilon_{\rm xc}^{\rm HEG}(n)|_{n=n(\vec{r})} \tag{1.33}$$

$$v_{xc}^{\rm LDA} = \frac{d}{dn} \varepsilon_{\rm xc}^{\rm HEG}(n)|_{n=n(\vec{r})}, \tag{1.34}$$

where $\varepsilon_{\rm xc}^{\rm HEG}(n)$ is the xc energy per unit volume of the homogeneous electron gas (HEG) of constant density n.

The correlation functional is obtained by a simple parametrized form fitted to several densities calculated by using quantum Monte Carlo simulations of Ceperley and Alder [12] on homogeneous electron gases. The most common parametrizations in use are PZ81 [13], PW92 [14].

The LDA is exact for an homogeneous electron gas, so it works well for systems in which the electron density does not vary rapidly, thus being well suited for the description of crystalline simple metals. Some results, provided within the L(S)DA approximation, are found to be in very good agreement with experimental data, such as determining molecular properties - equilibrium structures, harmonic frequencies, charge moments [15]. This approach, being successful for some systems, can also lead to failures; some of these are the wrong unstable prediction for stable negative ions (H^-, O^- and F^-), underestimation of semiconductor's band gaps, overestimation of hydrogen bonds.

The generalized gradient approximation (GGA), another well known functional and a simple extension of the LSDA

$$E_{\rm xc}^{\rm LSDA}[n_\uparrow, n_\downarrow] = \int d^3r\ n(\vec{r})\varepsilon_{\rm xc}[n_\uparrow(\vec{r}), n_\downarrow(\vec{r})], \tag{1.35}$$

where $\varepsilon_{\rm xc}(n_\uparrow(\vec{r}), n_\downarrow(\vec{r}))$ is the exchange-correlation energy per particle for an electron gas of uniform spin densities $n_\uparrow$ and $n_\downarrow$, is of the form

$$E_{\rm xc}^{\rm GGA}[n_\uparrow, n_\downarrow] = \int d^3r\ f(n_\uparrow, n_\downarrow, \nabla n_\uparrow, \nabla n_\downarrow). \tag{1.36}$$

This functional differs from the LDA because ε depends, not only on the density, but attempts to incorporate the effects of inhomogeneities by including the gradient of the electron density, ∇n (semi-local method). GGA is more widely used in quantum chemistry, but LSDA remains the most popular way to do electronic-structure calculations in solid state physics.

Hybrid functionals are perhaps the most accurate density functionals in use for quantum chemical calculations and incorporate a portion of exact exchange from Hartree-Fock theory with exchange and correlation from other sources, such as LDA, or empirical results. An hybrid approach was introduced by Axel Becke [16] that concluded that a fraction of exact

exchange should be mixed with GGA exchange and correlation. The simplest functional form is

$$E_{\mathrm{xc}}^{\mathrm{hyb}} = aE_{\mathrm{x}}^{\mathrm{exact}} + (1-a)E_{\mathrm{x}}^{\mathrm{GGA}} + E_{\mathrm{c}}^{\mathrm{GGA}}, \tag{1.37}$$

where the constant a can be fitted empirically or estimated theoretically as $a \sim 1/4$ for molecules [17].

1.1.4 Expansion of the Kohn-Sham Wavefunctions

Plane-Waves

Plane-wave expansion of the Kohn-Sham wavefunctions takes advantage of the periodicity of extendend systems.For finite system calculations (atoms, molecules and clusters), this type of expansion can also be performed if using the supercell approach. This can be achieved by placing the system in a large enough unit cell, in order to avoid interactions between neighboring cells.

The Kohn-Sham wave-functions are written according to Bloch's theorem in order to ensure that the combination of basis orbitals, verifies the translational periodicity of the supercell. Thus,

$$\varphi_{\vec{k},n}(\vec{r}) = e^{\imath\vec{k}\cdot\vec{r}} \sum_{\vec{G}} c_{\vec{k},n}(\vec{G}) e^{\imath\vec{G}\cdot\vec{r}}, \tag{1.38}$$

where $\vec{k}$ is the wave vector, n the band index, and $\vec{G}$ are the reciprocal lattice vectors, of the form $\vec{G} = m_1\vec{b}_1 + m_2\vec{b}_2 + m_3\vec{b}_3$, with

$$\vec{b}_i = 2\pi \frac{\vec{a}_j \times \vec{a}_k}{\vec{a}_i \cdot (\vec{a}_j \times \vec{a}_k)}. \tag{1.39}$$

The electronic density is

$$n(\vec{r}) = \sum_{\vec{k},n} \sum_{\vec{G},\vec{G}'} f_{\vec{k},n} c^*_{\vec{k},n}(\vec{G}') c_{\vec{k},n}(\vec{G}) e^{\imath(\vec{G}-\vec{G}')\cdot\vec{r}} \tag{1.40}$$

where $f_{\vec{k},n}$ are the occupation numbers. Fourier tranforming the density, one gets

$$n(\vec{G}) = \sum_{\vec{k},n} \sum_{\vec{G}'} f_{\vec{k},n} c^*_{\vec{k},n}(\vec{G}' - \vec{G}) c_{\vec{k},n}(\vec{G}'). \tag{1.41}$$

Two convergence parameters need to be adjusted for periodic condition calculations. One of these are the Brillouin zone sampling. Physical quantities require integration over the Brillouin zone in the supercell method, hence to evaluate these integrals computationally, a weighted sum over special $\vec{k}$-points (irreducible representative $\vec{k}$ vector) is performed. The second convergence parameter is the cut-off radius of the density in reciprocal space, to truncate the sums over the reciprocal lattice vectors. The cut-off energy is given by $E_{\text{cutoff}} = G_{max}^2/2$, where G_{max} is defined as the radius of the sphere that contains all plane-waves, $V_{\text{sphere}} = (4\pi/3)G_{\text{max}}^3$.

Though the use of supercells may be a natural choice in solid state physics, one needs to be aware of some consequences. Due to the long-range interaction between a charged cluster and its periodic images, the supercell approach is restricted to neutral systems. Thus, calculations performed on charged periodic systems must be considered with care and different methods can be applied in order to solve these problems [8]. The study of defects, by using the supercell approach, also needs to be done with some care. For such studies, this technique represents an infinite array of defects separated by lattice vectors and surrounded by the host species. When the lattice vectors are not large enough, spurious effects can take place in the form of defect-image coupling through interactions. This can also be well accounted for when using the LDA functional. Due to the predicted underestimation of the band-gap in semiconductors by the functional, and for a non adequate sized supercell, mixing between defect-related gap states with the band extrema can lead to serious problems, especially when one intends to study charged defect levels and/or shallow levels [1].

Gaussian Basis Functions

Another form to solve the Kohn-Sham equations is by expanding the orbitals in a localized orbitals basis set

$$\varphi_n(\vec{r}) = \sum_i c_{n,i}\phi_i(\vec{r}) \tag{1.42}$$

with n labeling the electron state and i the label of the basis functions. The error of the approach is determined by the number of functions used and the suitability of the choice of these functions ϕ_i.

One common choice for the localized orbitals is gaussians multiplied by polynomials of the position vector

$$\phi_i(\vec{r}) = (x - R_{ix})^{l_1}(y - R_{iy})^{l_2}(z - R_{iz})^{l_3} e^{-a_i|\vec{r}-\vec{R}_i|^2}, \tag{1.43}$$

with $l_i \geq 0$ determining the type of orbital (for example, $\sum_i l_i = 1$ is a p-orbital).

The charge-density is then calculated by

$$n(\vec{r}) = \sum_{i,j} b_{ij}\phi_i^*(\vec{r})\phi_j(\vec{r}) \tag{1.44}$$

$$b_{ij} = \sum_n f_n c_{n,i}^* c_{n,j} \tag{1.45}$$

where f_n is the occupancy of the n state and b_{ij} the density matrices [18].

Within this approach, one can infer that finite system calculations can overcome some disadvantages that periodic calculations endure, mainly computational cost when compared to using a supercell approach. Nevertheless, this method can have its shortcomings when one intends to evaluate a finite cluster of atoms, such as [19]

- the total electric dipole may depend on the location of the defect
- cluster surfaces must be saturated, otherwise the surface states from dangling bonds could interfere with gap states from the defects
- existence of defect-surface interaction is dependent on the size of the cluster

Real Space

Within the scheme of real space calculations, functions are not expanded in a basis set, but are sampled in an uniform, real-space mesh. Convergence of the results has, therefore, to be checked against the grid spacing [8].

The study of finite systems, molecules, or clusters, may be performed without the need of a supercell, simply by imposing that the wave-functions are zero at a surface far enough from the system. Infinite systems, such as a bulk material, can also be studied by defining the appropriate cyclic boundary conditions.

Just as all the approachs, real-space methods suffer from a few drawbacks, which can be minimized by reducing the grid-spacing. These are,

- most of the implementations are not variational - a total energy lower than the true energy may be found, and if so, when reducing the grid-spacing the energy can actually increase
- the grid can break symmetries that the system possesses, leading to the artificial lifting of some degeneracies.

1.2 Silicon Nanocrystals

1.2.1 Gap Width as a Function of the Nanocrystal Size

Silicon nanocrystals and similar nanostructures have been intensively studied in the last years due to their interesting quantum confinement properties. The strong spatial localization of electrons and holes in Si NCs can enhance radiative recombination rates and give rise to luminescence [20].

In the bulk regime, silicon has an indirect, low energy gap of 1.1 eV, in the infra-red region [21]. As the size of the Si specimen decreases, reducing into a finite sized material (Si nanocrystal), this energy gap tends to widen, driving the lowest occupied molecular orbital (LUMO) and highest occupied molecular orbital (HOMO) further apart and ultimately giving the small nanocrystals a direct gap-like behaviour [22], discrete energy spectra, an important feature for optoelectronic and photonic applications. The greater the difference between the HOMO and the LUMO, more energy is needed to excite the nanocrystal, and therefore, more energy is released when the crystal returns to its fundamental state, resulting in a colour shift from red to blue of the emitted light, hence allowing for photoluminescence (PL) across the visible spectrum [23]. By this, one can infer that one of the main advantages of Si-nanocrystals (Si-NC) is the possibility for atomic manipulation, allowing the control over the conductive and optical properties of the material just by altering the size of the gap or its chemical composition.

Ab initio studies are needed to achieve a better understanding of the size dependence of optical processes in confined systems. Empirical approaches suffer from the transferability of the bulk interaction parameters to the confined system environment, thus affecting the optical gaps due to the quantum confinement changes in the self-energy corrections (corrections that correspond to those of the bulk). First principle studies, that had been limited to small sized crystals and had known problems of band gap underestimation by the

local and semi-local functionals, can now achieve more accurate results. The improvements are due to advances in electronic structure algorithms and computational infrastructures, and the gap problem can be overcome due to alternative formulations of optical gaps, adequate to apply to confined structures [24].

There are two distinct formulations for the optical gaps: the quasiparticle gap, ϵ_g^{qp}, which is the difference between the ionization energy (energy needed to remove an electron from the N-electron system) and the electronic affinity (energy gain when an electron is added to the N-electron system) [25]; and the excitonic or optical gap, ϵ_g^{opt}, which accounts for an electron-hole pair bound by E_{Coul}. Therefore, the form of the optical gap is

$$\epsilon_g^{opt} = \epsilon_g^{qp} - E_{\mathrm{Coul}} \tag{1.46}$$

where E_{Coul} is the Coulomb exciton binding energy [26]. Both these components are different from their bulk values in small nanoclusters due to quantum confinement [27].

For an N-electron system, the quasiparticle gap, ϵ_g^{qp}, without account of the direct interaction of electron and hole, can be expressed in terms of the ground state total energies E of the $(N+1)$-, $(N-1)$-, and N-electron systems, as [26]

$$\epsilon_g^{qp} \quad = \quad E(N+1) + E(N-1) - 2E(N) \tag{1.47}$$

thus requiring the self-consistent solutions of three different charge configurations.

In the bulk limit, Eq. 1.47 is simply the difference between the Kohn-Sham eigenvalues of the lowest unoccupied and the highest occupied states.

Excitonic Coulomb and exchange-correlation energies need to be included if one wants to compare results with experimental absorption data. Quantum confinement in nanostructures enhances the bare exciton Coulomb interaction, also reducing the electronic screening, so that the exciton Coulomb energy can be comparable to the quasiparticle gap. If using an "exact" exchange-correlation functional within DFT and in the case of bulk silicon, the quasiparticle gap should be close to the optical gap because excitonic effects are small. Since LDA (or GGA) is not exact, the optical gap limit is not met [28].

The Coulomb exciton energy, of Eq. 1.46, needs to be evaluated accurately, hence there have been several techniques in order to obtain this value for quantum confined systems.

Effective mass approximations (EMA) cannot account adequately for such energies because the microscopic features of the electron-hole wavefunctions, inside the confined system, are neglected and the wavefunctions are constrained to vanish outside the crystal, instead of decaying smoothly into the vacuum.

Other calculations using the bulk dielectric constant, or reduced dielectric constant, of a quantum system for all the electron-hole distances are also not adequate, since and in the case of confined systems, the dielectric screening is different at increasing/decreasing respective length scales. One of the most direct and adequate approach can be obtained by using *ab initio* pseudowavefunctions calculations, though these can be computationally very demanding [24]. Therefore and within this framework, the exciton Coulomb energy can be written as

$$E_{\text{Coul}} = \int\int \epsilon^{-1}(\vec{r_1}, \vec{r_2}) \frac{|\psi_e(\vec{r_1})^2||\psi_h(\vec{r_2})^2|}{|\vec{r_1} - \vec{r_2}|}\, dr_1 dr_2 \tag{1.48}$$

with ψ_e and ψ_h being the electron and hole wavefunctions, respectively and $\epsilon^{-1}(\vec{r_1}, \vec{r_2})$ the inverse of the microscopic dielectric matrix. The evaluation of the matrix is what contributes for the demanding computational task of the pseudowavefunctions calculations.

The optical absorption spectra can be computed using a linear response theory within the adiabatic time-dependent local-density approximation (TD-LDA); this formalism allows the inclusion of the electronic screening and correlation effects, which determine exciton binding energies, to be evaluated within an *ab initio* framework. This technique is developed to include the proper representation of excited states [29], being this an extension of the ground state density-functional formalism. Compared to other theoretical methods, such as the many-body perturbation theory (MBPT) involving the Bethe-Selpeter equation, the TD-LDA approach requires considerably less computational effort and can be applied to much larger systems. However, the choice of the right xc-approximation with respect to the given excited state property is crucial. Therefore, MBPT comes as a well established and intuitive formalism, based on Green functions, where quaisparticle energies appear as a natural domain and accounting for a better behaved description of excited states.

1.2.2 Doped Silicon Nanocrystals

Another form of controlling the electronic and optical properties of Si-NC is by introducing impurities in the material [30]. Doped nanocrystals may emit light different than those emitted by pure NC, indicating that the impurity level affects the absorption and photoluminescence spectra.

The presence of single donor and acceptor states can lower the energy gap of the pure Si-NC [32, 21], whereas deep defects may degrade device performance. Hence, and since the new generation of optoelectronic devices is being drawn towards the nanometre, it becomes crucial to understand the properties of dopants in confined systems [32].

Phosphorous and Boron are the most studied dopants in Si (as they are easier to incorporate) and thus their binding energies, as shallow impurities, are well established for the bulk Si semiconductor. The binding energy for the substitutional donor, P, is of the order of 33 meV, and the acceptor energy for B is 45 meV [33]. Hence these impurities in bulk Si introduce defect energy states close to the conduction and valence band, respectivly, enabling thermal excitation of the charge carriers, thus enhancing the conductivity of the material and altering the respective transport properties [34]. Reducing the dimensionality of the system, these electric levels start to deepen into the mid gap, being this an evidence of how the size of the nanocrystal affects the localization of the electric states [21]. The combined effects of both quantum confinement and weak screening thus transform well established shallow impurities of the bulk, into deep levels in the nanocrystals [21].

It is worth mentioning that doping in nanostructures is more problematic than in bulk materials. One of the main difficulties is the control over impurity concentration and precise positioning, because of the out-of-phase relation of impurity concentrations between nano and bulk-sized materials - a small amount of dopant atoms can correspond to higher impurity concentrations in a nanomaterial [35]. Increasing dopant concentration results in distinct changes in the photoluminescence properties due to the influence on the mobility of the charge carriers [36]. In fact, it has been established that the emission intensity of NCs with low concentration of P (B) impurities is higher (lower) than for pure NCs, resulting that higher impurity concentration may suppress the luminescence intensity [30].

Another problematic issue arising in doped nanomaterials is the self-purification. One of the major issues, regarding this fact, is the possible deactivation of the functionalization

properties of impurity atoms that can be expelled or segregated to the surface of the material due to energetic and kinetic processes, that result from the effects of the confined dimensions [35].

Quantum Confinement Effects *vs* Weak Dielectric Screening

Several works intend to explain dopant localization in NCs on the basis of two theories. Experimental data tend to regard this feature based on quantum confinement effects, whereas some theoretical calculations seem to show that dopant localization also results from the decrease of the dielectric screening. Both these theories are related to the size of the crystal.

Based on reference [37], the electron wavefunction localization should be explained differently for distinct NC radius R:

1. for $R > 3.5a_B^{eff}$ nm, the reduction of the dielectric screening determines the localization
2. for $R < a_B^{eff}$ nm the influence of the confining surface potential prevails over the dielectric screening
3. for intermediate size ranges, both dielectric and quantum confinement contribute to the electron localization

with $a_B^{eff} = 1.67$ nm being the effective Bohr radius of the bulk system.

The measure of how strongly the defect electron interacts with the impurity atom can be determined by its binding energy. Taking as example the case of a P-dopant, this energy is calculated by the energy required to ionize a P-doped Si nanocrystal by removing an electron, IP_d, minus the energy gained by adding the electron to a pure Si nanocrystal, EA_p. Thus,

$$\begin{aligned} IP_d &= E_d(N-1) - E_d(N) \\ EA_p &= E_p(N) - E_p(N+1) \end{aligned} \tag{1.49}$$

where E_d and E_p is the ground state total energy of the N electron system for doped and pure Si, respectively. The binding energy is determined by calculating the difference

between these quantities [36]

$$E_B = IP_d - EA_p. \tag{1.50}$$

This definition of the binding energy for confined systems is not similar to the bulk's definition of such quantity. In the bulk regime the binding energy is defined as the difference between the dopant electron level and the conduction band. In nanocrystals this definition is not valid since an excited electron will be confined by the physical size of the crystal and will continue to interact strongly with the impurity atom [36].

It has been observed in ref. [34] that for NCs with diameters larger than 2 nm, the binding energy tends to decrease as the P atom moves towards the surface. This is due to the defect wavefunction becoming more delocalized around P, leading to a Coulomb energy loss between the impurity and the electron, hence making the centre of the nanocrystal energetically more stable. For Si crystals less than 2 nm in diameter, the binding energy is higher close to the surface, thus P segregates to the surface. The binding energy and the stress induced by the dopant are responsible for determining the defect position in the crystal with respect to the size regime [34]. These results can be compared with the ones obtained by Melnikov *et al.* [36], with Si nanocrystals sizes ranging from 0.8 nm to 2.4 nm in diameter. It was inferred that the choice of the P site does not have a strong influence on the binding energies; nevertheless a minor difference was found - the centre position is more stable than the surface position by about 0.6 eV. It was also suggested by Zou *et al.* [38] that, in doped silicon nanocrystals, the most significant physical effect that determines the positioning of the defect level is the reduced screening of the impurity potential that leads to the large donor and acceptor binding energies (not allowing for the formation of shallow impurities in confined systems [36]); the screening inside the nanocrystal is less effective than long range screening in bulk Si.

Studying the ionization energies with respect to the radii of the nanocrystals, Melnikov *et al.* [36] inferred that these were unchanged throughout the studied range of crystals, being this value approximated to the bulk's value (4.2 eV). Hence, conclusions withdrawn from here are that the ionization energies do not exhibit a quantum confinement behaviour, but this can be attributed to a strong electron-impurity interaction [36] due to the weak screening and strong localization around the defect.

The hyperfine splitting (HFS), that results from the interaction between the electron

spin of the defect level and the nuclear spin (which is directly related to the dopant electron density localized on the impurity site), is observed to be very large for small nanocrystals, due to a strong localization of the electron around the impurity. It has also been found that the HFS increases with respect to the bulk [36], which suggests that the screening dielectric constant of the NCs is not equal to the dielectric bulk value, $\varepsilon_{bulk} = 11.7$ eV [37].

Ab-initio pseudopotential calculations [34] have also concluded that the P defect in Si-NCs can be well described by the hydrogenic system, using the model calculation of a hydrogen atom confined in a quantum well ("dielectric box"), V_0. This is plausible because the defect wave function, ψ, has a functional form similar to the $1s$ orbital, where

$$\psi \sim \exp\left(-r/a_B^{eff}\right) \tag{1.51}$$

being a_B^{eff} the effective Bohr radius that is dependent on the nanocrystal size ($a_B^{eff} \sim 1.67$ nm in the bulk system [37]).

It was found by Chan *et al.* [34] that the effective Bohr radius decreases as the NC size is reduced; but, for very small crystals, $R \to 0$, the Bohr radius tends to converge to ~ 0.2 nm. The authors concluded, after fitting the data that was obtained to an effective mass model, that the depth of the potential well is dependent on the nanocrystal radius, suggesting that V_0 represents the effect of quantum confinement on the wavefunction. Thus, in the range of small sized crystals, the kinetic energy of the defect electron increases due to the reduction of the dielectric screening; therefore the quantum well tends to deepen such that it can confine the electron. Whereas, when the limit of the bulk regime is met, the well vanishes.

Dopant Contenders

Possible contenders for shallow donors in silicon nanocrystals can be considered with elements belonging to the alkali group (I) (Li, Na and K) as these have lowest ionization energies. For acceptor-dopants, attention can be drawn to the first three elements, with highest electronic affinities, belonging to the halogen group (VII-B) (F, Cl and Br).

Works regarding the usage of halogen elements as dopants have already been carried out in the diamond lattice. A recent one, accomplished by Yan *et al.* [39], shows that doping diamond with these elements becomes more difficult as one goes down the halogen column of the periodic table, due to the increase of the respective formation energies. In

spite of this difficulty, it has been seen that substitutional doping is more favourable. In principle, it is possible for these elements both to accept and donate electrons from and to the diamond lattice, respectively, as it has been shown in reference [39]. Though F dopant (substitutional or interstitial) may act as an acceptor, doping diamond with Cl, either using any of the two sites, or with substitutional Br, enables a donor state in the lattice. Interstitial F is a shallow acceptor, thus being a good candidate for p-type conduction for the diamond lattice, whereas interstitial Cl introduces deep levels in the gap. Being difficult to dope with interstitial Br, due to the large values of the formation energies, it has not yet been possible to gather information regarding the respective electrical levels.

Studies also show that Li and Na in the diamond lattice are unlikely to produce n-type materials due to deep levels these introduce in the band gap. Calculated donor levels (for interstitial sites) were obtained at $E_c - 0.1$ eV [40] and $E_c - 0.6 \pm 1$ eV [41] for Li and $E_c - 0.3$ eV [40] and $E_v + 3.6$ eV [41] for Na. Although Li might be considered a good candidate for donor doping, it is insoluble, mobile (during typical growth and annealing conditions) and it is likely to form complexes with other impurities, hence inactivating any possible electrical levels that could eventually occur [41]. Nevertheless, it has been registered that after Li implantation, n-type material can be produced, but a reduction in the conductivity may occur when annealing up to 600°C [42].

Li is a fast diffuser in diamond, just as it is in Si, and the possibility of matching these two elements can enable outstanding applications. An example of this coexistence are the Li-ion batteries, with Si being one of several compounds proposed to replace graphite. However, commercial applications are not yet viable due to problems that are encountered in silicon bulk-based materials, such as large volume change during Li uptake and capacity loss due to decrepitation, resulting in a reduction in the effective capacity during cycling [43]. These problems can be overcome with nano-sized materials, such as Si nanotubes or nanowires, because of their outstanding mechanical properties, allowing for these to better support huge amounts of stress, thus avoiding cracks that may occur after repeated charging and discharging cycles [35]. Another advantage is the increase of the surface area of the anode, due to the large surface-to-volume ratio characteristic of the nanomaterials, allowing for a more effective uptake by the cathode.

Another well established shallow impurity for the bulk Si (besides the already mentioned P and B) are the thermal double donors (TDD). Thermal double donors are

formed by annealing Czochralski-grown, oxygen-rich, Si at temperatures ranging between 350°C and 500°C. Their levels are found to be around $E(0/+) = E_c - 0.07$ eV and $E(+/++) = E_c - 0.15$ eV [44] for bulk Si. Small oxygen chains, aligned along [110], can migrate through the lattice more easily than interstitial O, due to lower migration barriers; hence rapid chain diffusions enables long chains to grow rapidly. The lowest energy chain is found to belong to the O_∞−2NN model, where oxygen is bonded to second neighbour Si atoms in two parallel chains [45]. It has been seen in reference [45], that the infinite chain model is insulating, while for the finite chain this is not true. For the finite chain an occupied state edges the conduction band due to the end regions. The origin of donor activity is the result of the topological defect at the interfaces between two oxygen configurations, either over-coordinated oxygen species or divalent oxygen together with a Si dangling bond.

Chapter 2

Computational Method

The calculations were divided in two sections. The first section is based on the study of the gap width as a function of the nanocrystal size. The aim of this study was to try to reproduce theorectical data from relevant literature and confirm that the convergence parameters defined in the codes were adequate for the present studies. The second section is based on the study of the electronic properties of doped silicon nanocrystals, namely the defect level localization within the gap.

In order to evaluate the required quantities two density functional based codes (DFT) were used: AIMPRO (*Ab-initio* Modelling Program) [46] and Octopus [47], where with Octopus, results were obtained only for the first set of calculations.

AIMPRO

AIMPRO can run in two distinct modes, the supercell mode, where periodic boundary conditions simulates a bulk system by expanding the charge density in plane-waves, and the cluster mode, where it is required the use of Gaussian (localized) basis-sets in order to expand the same property.

The usual way to expand the charge density and potential terms has been with plane waves as these fit naturally with periodic boundary conditions. As already mentioned in 1.1.4, there are disadvantages with the use of plane wave expansions, being the major of these problems, the need of an extremely large number of functions when studying localized problems.

As the dynamics of a system is described by the Schrödinger equation, a differential equation, appropriate boundary conditions should be imposed [48]. Since grown freestanding Si-NCs produced by plasma decomposition of silane are H-passivated at the surface, a

real-space, non-periodic, calculation is also therefore the most appropriate mode of calculation to apply to such systems. This also applies to surface oxidized NCs that are also reported.

For these two mentioned reasons, localized-based functions were therefore chosen to evaluate the desired quantities for the H-passivated silicon nanocrystals.

For the two sets of studies, the exchange-correlation interaction was accounted for by the the LDA, using the Padé approximation to the PW92 functional [49, 14]. The core states were replaced by norm-conserving pseudopotentials of the Hartwigsen, Goedecker and Hutter [50] type, that are a optimal analytical integration in real-space using Gaussian basis sets.

For the gap convergence study, the valence states and electron density were represented by a set of atom-centred s-, p-, and d-like Gaussian functions, and the Kohn-Sham states were expanded with the help of a set of contracted basis: C44G* for Si and H. Uncontracted basis-sets are defined as a set of exponents are completely free to vary during a run, while the contracted basis-set is a set of exponents and coefficients used to generate fixed combinations of these functions. The use of contracted basis, on atoms, can lower the computational cost without significant loss of accuracy. The basis nomenclature, C44G*, describes the nature of the material for which the basis are optimised (carbon) and the number of the fitting functions - two sets of four Cartesian Gaussian Orbitals of different exponents that are combined into fixed functions (one *s*- and three *p*- polynomial combinations), with polarization functions, * (addition of a *d*-type function), in order to improve the description of the Si atoms in the nanocrystal environment [18].

To perform the calculations of the doped systems extra care was required and so convergence tests were performed on doped nanocrystals with 124 Si atoms, passivated by 96 hydrogen atoms, applying several types of wavefunctions and charge density functions. The purpose of these tests was to verify the best basis to be applied for NCs with 304 Si atoms and passivated with 168 hydrogen atoms, which are experimentally feasible size ranges - about 2.25 nm in diameter.

The dopants were chosen, as already mentioned, according to their electron shell properties, namely those with lowest ionization energies (Li, Na, K) and those with highest electronic affinities (F, Cl, Br) - fig. 2.1. These were placed at the centre of the crystal (centre of the tetrahedral cage), at the interstitial site. P and B dopants were also stud-

ied, but positioned in the substitutional site, this being the most stable site for these two dopants [21].

The TDD was also calculated in order to compare results and establish the levels in the nanocrystal regime. It was chosen, amongst a family of at least 17 double donors, a thermal double donor characterized by a chain of O_5 atoms placed interstitially along [110] - fig. 2.2.

Valence states and the electron density for Si, the halogens and the substitutional dopants, were represented with the help of s, p and d-like Cartesian-Gaussian functions. For the interstitial donors (alkalis) and for H, these were described by s and p-like Cartesian-Gaussian functions, and the oxygens were depicted by s and d-like functions.

Uncontracted and contracted wavefunction basis-sets were also used for the three species involving the NC (Si, H and the dopants). The usage of functions was made according to the following scheme:

- for Si and H contracted basis was used (C44G*)
- for the remaining species uncontracted basis-sets were employed
  - for the interstitial dopants (the three donors, Li, Na and K and the three acceptors, F, Cl and Br) basis-sets, with angular momenta up to p on four exponents - pppp, were used
  - for O the dddd basis-sets was employed
  - the two substitutional dopants, P and B, were converged with ddpp and pdpp basis-sets, respectively.

The NCs were fully relaxed, including the outer cores of the hydrogens. The crystals with interstitial dopants preserve the same symmetry as the pure crystal, T_d, while in the NCs with substitutional dopants the symmetry is lowered to the trigonal symmetry, C_{3v}. The O_5 chain merged within the Si nanocrystal also reduces the high symmetry of the NC to C_{2v} symmetry.

Octopus

For cluster runs in AIMPRO, the default functional is the LDA functional. The GGA to the exchange-correlation potential is not available in the cluster mode. So, in order

to compare results between the local and semi-local functional and to avoid plane-wave calculations (where the GGA is provided within this mode), a real space code, Octopus, was also used. This program materializes the main equations of density-functional theory in the ground state and of time-dependent density-functional theory (TD-DFT) for dynamical effects.

Calculations, within Octopus, were hence initiated for the undoped silicon crystals, with different size ranges, applying LDA (Slater exchange and Perdew and Zunger Modified correlation [13, 51]) and GGA-PBE [52, 53] to represent the exchange-correlation interaction. Troullier and Martins norm-conserving pseudopotentials [54] (TM) were used as the effective potential.

As already discussed in subsection 1.1.4, and within the scheme of real space calculations, functions are represented by their value over a set of points in real space, hence the convergence parameters have to be checked against the grid spacing. Octopus, by default, allows for the use of equally spaced grids - points are distributed in a uniform grid, which means that the distance between points is a constant for each direction. In this scheme, the separation between points, or spacing of the simulation, is a critical value. When the separation becomes large, the representation of functions get worse and when it becomes small the number of points increases, thus increasing memory use and calculation time. This value is equivalent to the energy cut-off used by plane-wave representations.

A finite domain of the real space to run the simulations need to be selected (simulation box). This option optimizes the shape of the box to minimize the number of points and can be set accordingly to the geometric configuration of the system. Therefore, for the simulation box, the default option was choosen (minimum), which constructs a simulation box by adding spheres created around each atom of radius R.

By default Octopus assumes zero boundary conditions, that is, wavefunctions and density are zero over the boundary of the domain. This is the natural boundary condition when working with finite systems and thus, for this case the choice of an adequate box size is crucial. If the box is too small the wavefunctions will be forced to go to zero, but if the box is too large, a larger number of points is needed, increasing computational resources as well.

Convergence tests were performed with different radius of spheres and spacing between the points and checked against the differences between the total energies and re-

spective eigenvalues of six different sized crystals (Si29H36H, Si35H36, Si78H64, Si87H76, Si147H100 and Si304H168). Convergence was attained for radius of $R = 3.5$ Å and spacing of 0.23 Å for the smallest crystal, 0.30 Å for the biggest crystal, and 0.25 Å for the remaining systems.

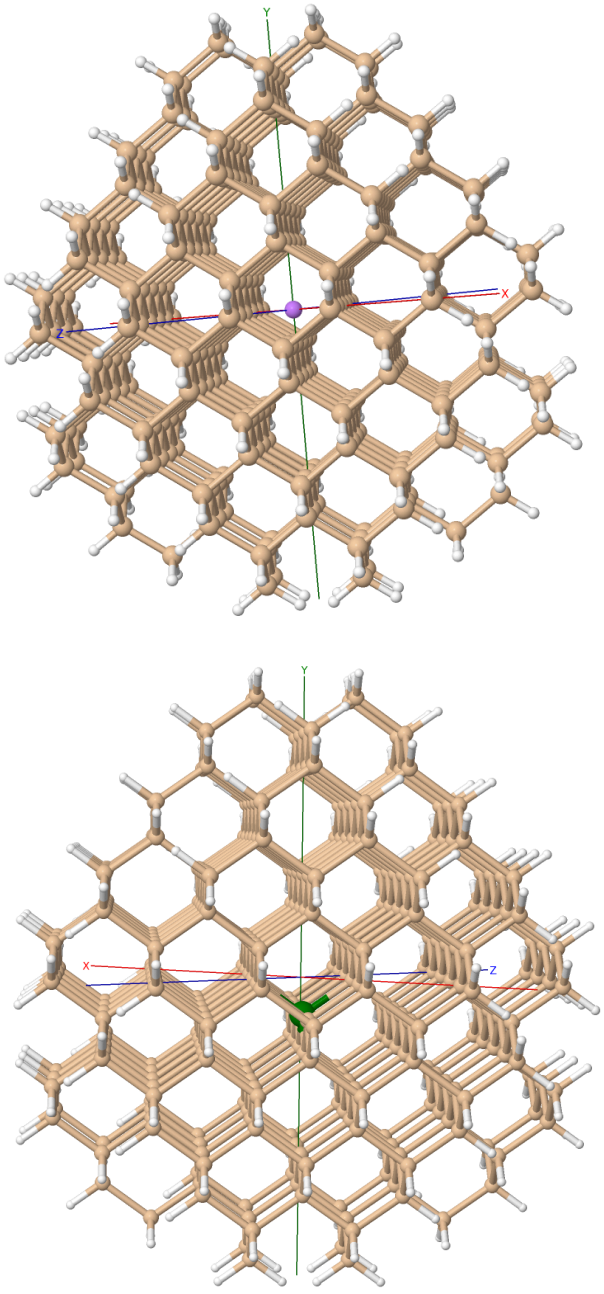

Figure 2.1: Hydrogen-saturated spherical Si nanocrystal doped with an interstitial defect (purple) - first figure and with a substitutional dopant (green) - second figure.

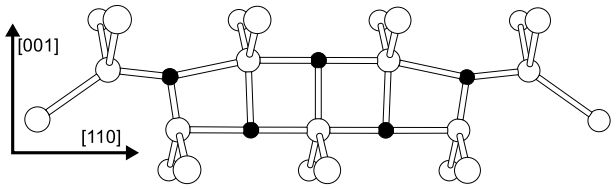

Figure 2.2: Representation of the O_5 thermal double donor chain in the Si nanocrystal. Red and black balls represent the O and Si atoms, respectively. Distance lengths are defined in nm.

Chapter 3

Results and Discussion

3.1 Gap Convergence of Silicon Nanocrystals

Different sized, spherical nanocrystals were used in order to reproduce the confinement gap effects, the sizes of the crystals ranging from the smallest crystal - 1.03 nm to the biggest - 2.25 nm in diameter; all of these spherical systems were passivated by hydrogens (hydrogen terminated Si-NC) to induce the gap-size dependence. The diameters were calculated within the core of the silicon atoms (disregarding the H atoms) and using the following relation

$$R_{\text{adius}} = \left(n_{\text{atoms}} \frac{3}{n_{\text{unit}} 4\pi} a_0^3 \right)^{1/3} \tag{3.1}$$

where the lattice parameter, a_0, is obtained by calculating the average bond lengths of all the crystals under study, hence $a_0 = 5.38$ Å, and n_{unit} is the number of atoms contained in the unit cell of bulk silicon (2 atoms per unit cell).

Two sets of calculations were made in order to study the gap with respect to the crystal size: quasiparticle gap and the single-particle band gap (LDA or GGA gap) - table 3.1. The first set is defined as being the difference between the ionization potential and the electronic affinity, as already mentioned in 1.2.1 - fig. 3.1. Hence,

$$\begin{aligned} IP &= E(N) - E(N-1) \\ EA &= E(N+1) - E(N) \end{aligned} \tag{3.2}$$

where E is the ground state total energy of the neutral, E(N), positively charged, E($N-1$), and negatively charged, E($N+1$), electron system. The so called quasiparticle gap, ϵ_g^{qp} is

obtained by

$$\epsilon_g^{qp} = EA - IP, \tag{3.3}$$

which includes the quasiparticle corrections for systems with spatial confinement.

The usual single-particle band gap is defined as the eigenvalue difference between the lowest unoccupied and the highest occupied orbitals, LUMO and HOMO respectivly.

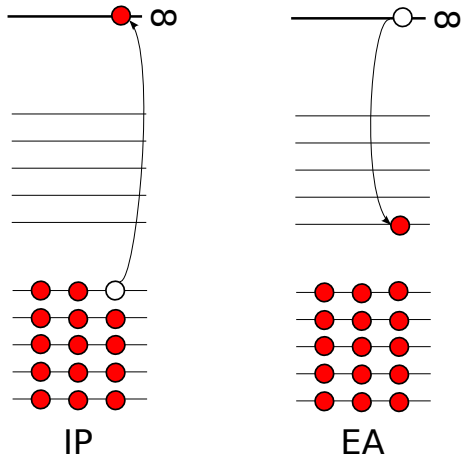

Figure 3.1: Representation of the ionization potential and electronic affinity

What is observed, for the different gap calculations, is that as the size of the cluster increases, the gaps tend to decrease. This can imply that the discrete spectra for small clusters evolves Size dependence of the quasiparticle and LDA band gaps are shown in figs. 3.2 and 3.3. Both gap values are enhanced with respect to the bulk values and are inversely proportional to the Si-NC diameter as a result of quantum confinement.

In table 3.1 the results of the two sets of calculations can be observed. The LDA gap width is about half the size of the quasiparticle gap. These latter calculations neglects the effects of the Coulomb attraction between the electron and the hole [55], this being one of the reasons why the quasiparticle gap is much bigger than the LDA gap. The fact that the local functional tends to underestimate the difference between the LUMO-HOMO eigenvalues also accounts for the gap width differences.

To compare results by using a semi-local functional, GGA was used for the same group of different sized crystals - table 3.2. What can be observed is that the results are very similar to the ones evaluated by using the LDA functional, either for the quasiparticle gap or for the gap evaluated from the differences between the eigenvalues (being the GGA values slightly bigger than the LDA). The differences of the quasiparticle gaps between the

two functionals are about 0.2 eV, for the smaller systems, but, this is reduced to 0.1 eV for bigger systems, inferring that for the bulk limit the differences between the two functionals will be even smaller.

Ionization energies and electronic affinities are shown in fig 3.5 and compared to those of the bulk system, where $IP_{\text{bulk}} = 4.8$ eV and $EA_{\text{bulk}} = 4.1$ eV [28]. For small NCs, the electronic affinities are small in comparison with the ionization energies. As the radius increases, the IP gradually decreases and the EA increases. For the results obtained from AIMPRO and Octopus, the IP and EA scale with radius R of the nanocrystal as R^{-l}, with $l = 1.1$, in contrast to the scaling factors $l = 2$ predicted by simple effective-mass models. These results are in accordance with ref. [28] (see fig. 3.3) that presents a large set of calcluations using a real-space *ab initio* pseudopotential (TM) code.

Table 3.1: Comparison of the quasiparticle and the difference beteween the LUMO and HOMO eigenvalues (LDA gap) obtained from AIMPRO and Octopus calculations for different nanocrystal sizes. The diameter of the nanocrystal is obtained by measuring the core of Si atoms (disregarding the outer core of the passivation H atoms) - eq. 3.1.

Si atoms	Diameter (nm)	AIMPRO		Octopus	
		QP gap (eV)	L-H gap (eV)	QP gap (eV)	L-H gap (eV)
29	1.026	6.4435	3.9260	6.5760	3.7888
35	1.092	6.3033	3.9241	5.8142	3.7200
78	1.427	5.0181	3.1108	4.7147	2.8574
87	1.480	4.8371	2.9909	4.5659	2.7186
110	1.600	4.5824	2.8566	—	—
124	1.665	4.4415	2.7746	—	—
130	1.692	4.3291	2.7012	—	—
147	1.762	4.2981	2.7074	3.7560	2.4119
172	1.857	3.9941	2.5134	—	—
196	1.940	3.8322	2.3909	—	—
211	1.988	3.8654	2.4485	—	—
244	2.087	3.6978	2.3465	—	—
256	2.120	3.6053	2.2765	—	—
275	2.171	3.4883	2.1853	—	—
286	2.200	3.5070	2.2256	—	—
304	2.245	3.5334	2.2671	2.7908	1.8628

3.2 Doped Silicon Nanocrystals

In this section, we present a study of the electronic properties of Si nanocrystals doped with impurities. Impurities were chosen, based on their electronic features (Li, Na, K, F,

Table 3.2: Comparison of the quasiparticle gap and the difference between the LUMO and HOMO eigenvalues obtained by using the LDA and the GGA functional within Octopus calculations. The diameter of the nanocrystal is obtained by measuring the core of Si atoms (disregarding the outer core of the passivation H atoms) - eq. 3.1.

Si atoms	Diameter (nm)	LDA		GGA	
		QP gap (eV)	L-H gap (eV)	QP gap (eV)	L-H gap (eV)
29	1.026	6.5760	3.7888	6.7549	3.9394
35	1.092	5.8142	3.7200	5.9657	3.8658
78	1.427	4.7147	2.8574	4.8922	3.0276
87	1.480	4.5659	2.7186	4.7532	2.8845
147	1.762	3.7560	2.4119	3.8967	2.5797
304	2.245	2.7908	1.8628	2.9210	2.0268

Cl, Br), and for some, based on their well established behaviour in bulk silicon (P, B and O_5), in order to verify if these could create shallow levels in the gap. Until today, it has not yet been possible to establish which impurities can contribute for n-type and p-type silicon nanoparticles due to the issues with nano-sized materials. Therefore, we explore the possibility of finding shallow dopants in Si nanocrystals where confinement effects become more pronounced.

For the intrinsic Si crystal with diameter of 2.25 nm, the difference between the ionization potential, IP, and electronic affinity, EA, following the procedure defined in eq. 3.3, was found to be 3.53 eV.

For the doped crystals, we calculated the ionization energy for the donor defects and the electronic affinity for the acceptor impurities, with results shown in table 3.3. To obtain n-type doping, the donor levels have to lie slightly below the LUMO of the host's crystal, in order for the donor electrons to be easily ionized, even at room temperature. The same is true for acceptor levels, but these have to be slightly higher than the HOMO of the undoped Si, contributing with holes to the top of HOMO. For neither of these two cases, shallow defect levels were found, being all these located deeply within the gap - a representation of the levels can be found in fig. 3.6. The respective energy states were obtained by calculating

$$\begin{aligned} E_D &= IP_D - EA_p \\ E_A &= EA_A - IP_p \end{aligned} \tag{3.4}$$

where E_D and E_A are the donor and acceptor energy states, respectively, IP_D and EA_A

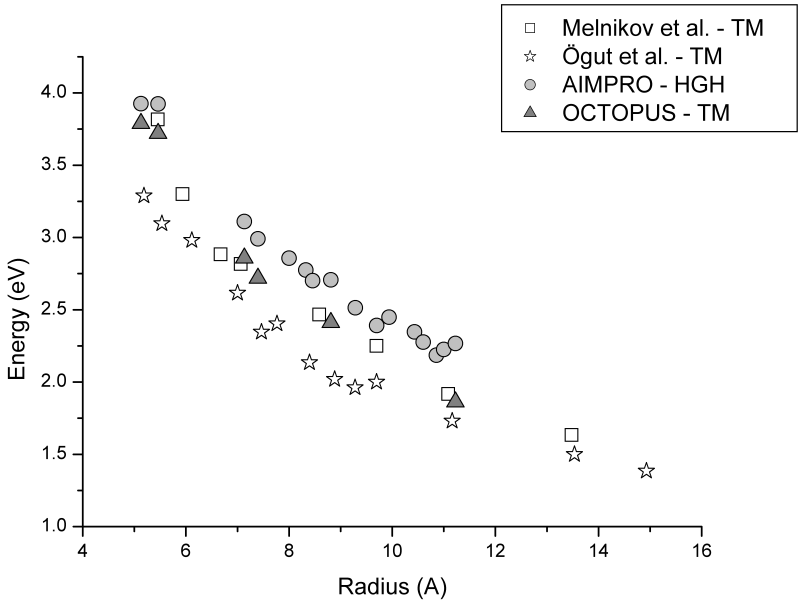

Figure 3.2: LDA gap of Si nanocrystals as a function of the radius of the nanocrystals, from calculations obtained from AIMPRO and Octopus and compared to results from references: Melnikov *et al.* [28] and Ögut *et al.* [24].

are the donor ionization potential and acceptor electronic affinity of the doped crystal, respectively, and IP_p and EA_p the ionization potential and electronic affinity, of the pure Si crystal, respectively.

The impurity donor states are approximately in the same energy range from each other, being the P level the one that lies deeper in the gap and distanced from the EA_p at about 1.55 eV. For the acceptor impurities, the deepest level distanced from the IP_p is 1.87 eV and is owed to the Br impurity, whilst the F impurity contributes with a defect level closest to the IP_p - 1.36 eV.

The well established shallow dopants (P, B and the TDD) for the bulk limit do not behave as so in the finite-size systems. These results are in accordance with references [21, 34, 36], and result from the lower Coulomb screening of the nanocrystals when compared to bulk silicon, hence enhancing the defect electron confinement that becomes dominant for the nanocrystal system [34].

In the presence of an interstitial impurity, placed at the centre of the crystal, the Si-Si surrounding cage undergoes a structural displacement. The bonds between the Si neighbours tend to expand in comparison to the pure crystal. The biggest displacement

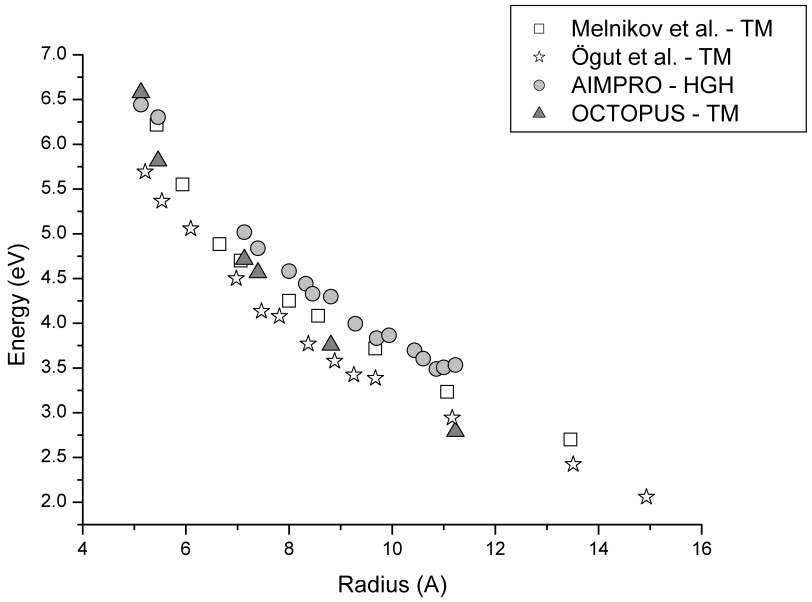

Figure 3.3: Quasiparticle gap of Si nanocrystals as a function of the radius of the nanocrystals, from calculations obtained from AIMPRO and Octopus and compared to results from references: Melnikov *et al.* [28] and Ögut *et al.* [24].

occurs for the K impurity, where the distance between the bonds expands by about 6.7% compared to the intrinsic Si-Si bonds. The lowest shift occurs for one of the halogen impurities, F, being this value around 0.6%.

For the substitutional defects, alteration of the bonds only occur around the impurity as well. For the P impurity, the difference between the P-Si bonds tend to be very similar to those of the pure relaxed Si nanocrystal - distortion between the bonds is an expansion of 0.2% and the Si-Si next neighbour bonds increases by 0.04%. The B dopant causes more impact upon the B-Si bonds - these shrink by about 11.6% compared to T_d Si bonds, with an increase of the next Si-Si neighbour bonds of about 1.7%. These results are very similar to calculations performed in reference [56], inferring that the amount of relaxation around the impurity is directly related to the impurity's valence properties (B being a trivalent and P a pentavalent atom) [56].

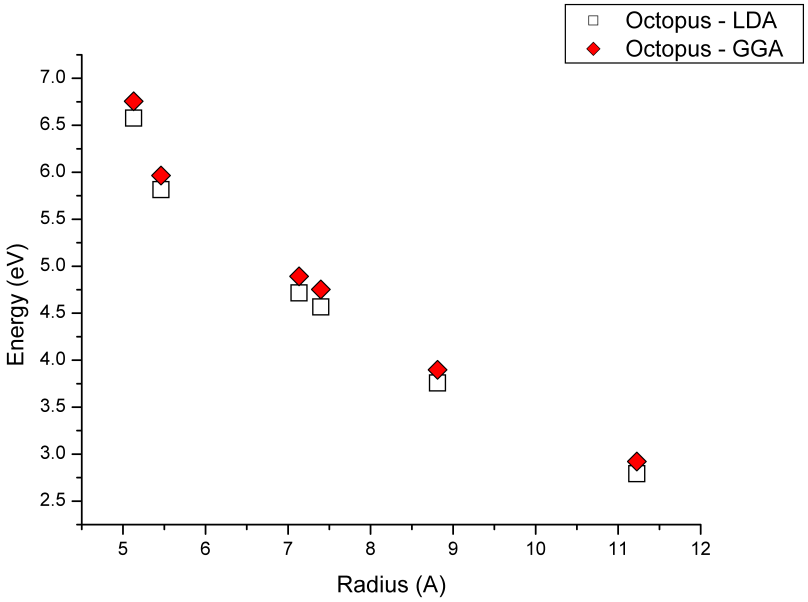

Figure 3.4: Quasiparticle gap of Si nanocrystals as a function of the radius of the nanocrystals, from Octopus calculations. Comparison is made between results of two different functionals: LDA and GGA.

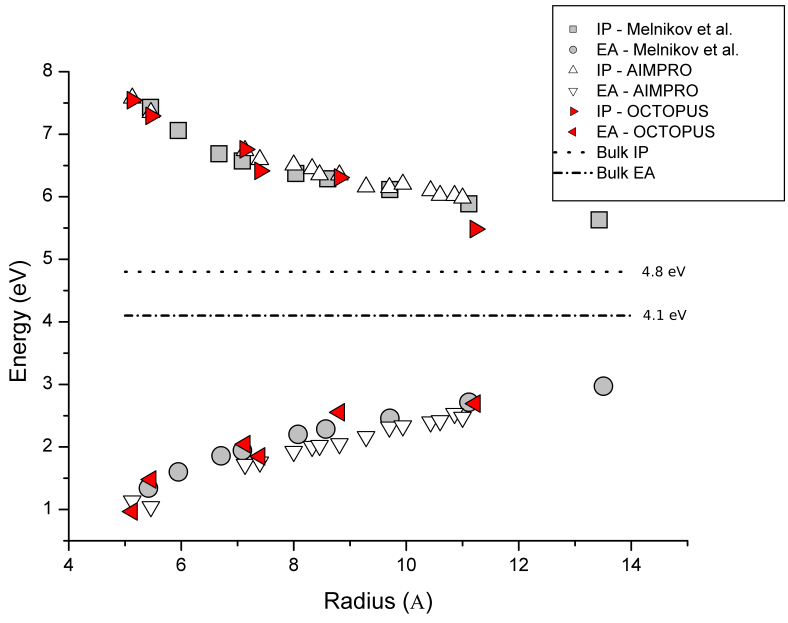

Figure 3.5: Ionization energies and electron affinities of Si nanocrystals as a function of the radius of the nanocrystals, from calculations obtained from AIMPRO and Octopus and compared to results from Melnikov *et al.* [28]. Respective bulk values are presented with IP=4.8 eV and EA=4.1 eV.

Table 3.3: Ionization potentials and electronic affinities for donors and acceptor Si impurities, respectively. For the TDD, only the first ionization potential was calculated. Defect energy state calculations were carried out on the Si304H168 crystal (2.25 nm of diameter). Values are given in eV.

	IP	EA
Si	-5.96	-2.43
	Interstitial Defects	
Li	-3.78	
Na	-3.78	
K	-3.82	
F		-4.60
Cl		-4.35
Br		-4.09
	Substitutional Defects	
P	-3.98	
B		-4.54
	Thermal Double Donor	
O_5	-3.82	

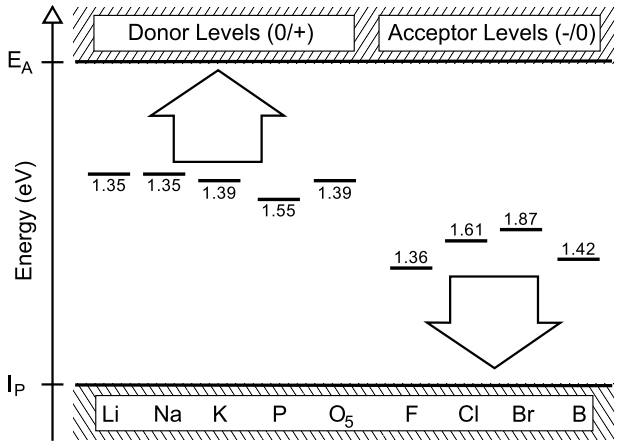

Figure 3.6: Energy levels of doped Si nanocrystals. The width of the quaisparticle gap for the Si304H168 crystal (2.25 nm of diameter) is 3.53 eV . All values are given in eV.

Chapter 4

Conclusions and Future Perspectives

4.1 Conclusions

Experimental works regarding controlled doping can become a difficult task, hence detailed studies based on this subject are still far from complete. As such, first-principles calculations may contribute with an helpful insight in the search for dopants with suitable electronic, optical or magnetic performance at the nanoscale. Hence, and within the density functional framework, calculations were carried out in order to obtain the P, B and O_5 chain impurity energy levels, well established bulk shallow impurities, and the alkali and halogen favourable contenders for n- and p-type doping.

In this dissertation work, it was demonstrated that no shallow energy levels were found for the doped silicon nanocrystals under study. At nanoscaled systems the dielectric screening is reduced in comparison to the bulk value, hence giving rise to a strongly localized defect state, due to the enhancement of the donor and acceptor binding energies, and the increase of the effective electron-impurity potential. The reduction of the screening effect enhances the defect level localization and transforms well known shallow impurity states of the bulk material into deep levels.

Considering the edge treatment, that is the origin of variety, the passivation of the dangling bonds is also known to be important for the electronic properties of hydrogen terminated silicon nanocrystals. Therefore, it was also seen, and in agreement with the cited theoretical literature, that the quasiparticle gaps, evaluated for these H-terminated systems, show a strong size dependence characteristic of the quantum confinement effects, and remain different from the corresponding bulk value. The same behaviour is also accounted for in the ionization potentials and electronic affinities of the same systems.

4.2 Future Perspectives

Core-Shell Transfer Doping

Altering the surface of the Si crystal with different species can alter its electrical properties. An example is surface oxidation. We know that Si natural oxide (SiO_2 or silica) appears when Si is exposed to an O-containing atmosphere by indiffusion of O_2 molecules through the SiO_2 network, until they meet the Si. Accordingly, the Si/SiO_2 interface advances through Si by replacing Si-Si bonds by Si-O-Si units [57].

SiO_2 has a wide gap of about 9 eV, and this presents an opportunity for *transfer doping* in core-shell nanostructures. Basically, a deep donor in SiO_2, with an occupied state lying above the LUMO level of the Si-NC core, will donate (or transfer) its electron to that LUMO level. Analogously, any deep acceptor level in SiO_2, with a level below the HOMO of the Si core, will remove an electron from the Si-NC HOMO level.

Finding a suitable dopant for the SiO_2 interface, which may contribute with a donor (acceptor) level slightly above (below) its LUMO (HOMO) state of the core is a tricky task, since the shell is amorphous and any foreign chemical species can occur in many configurations (some of them chemically inert). The mechanism governing tansfer doping is depicted in fig. 4.1.

These studies are still in their early stages. One of the most promising contenders for this study is the P dopant, which may replace a four oxidized Si atom, within the silica core. Because of its pentavalent nature, this impurity will give rise to a donor level - the question arises as if this will allow for transfer doping of an electron from the SiO_2 onto the Si-NC LUMO states.

Optical Properties

The study of optical excitations in hydrogen terminated silicon crystals is essential for understanding absorption and emission of light. Therefore the study of optical properties for the doped silicon nanocrystals can be thought of as an opportunity for such perspective. The calculations performed to obtain the electronic properties of the doped Si-NCs brought no expectation in finding impurity contenders for n- and -p type doping. But, a new perspective based on optical properties calculations can still unveil important properties for these confined systems, where underlying applications can emerge.

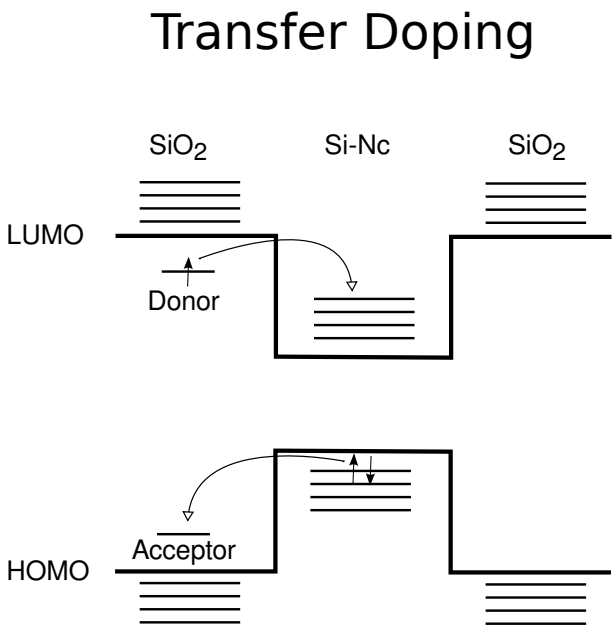

Figure 4.1: Schematics of transfer doping effects.

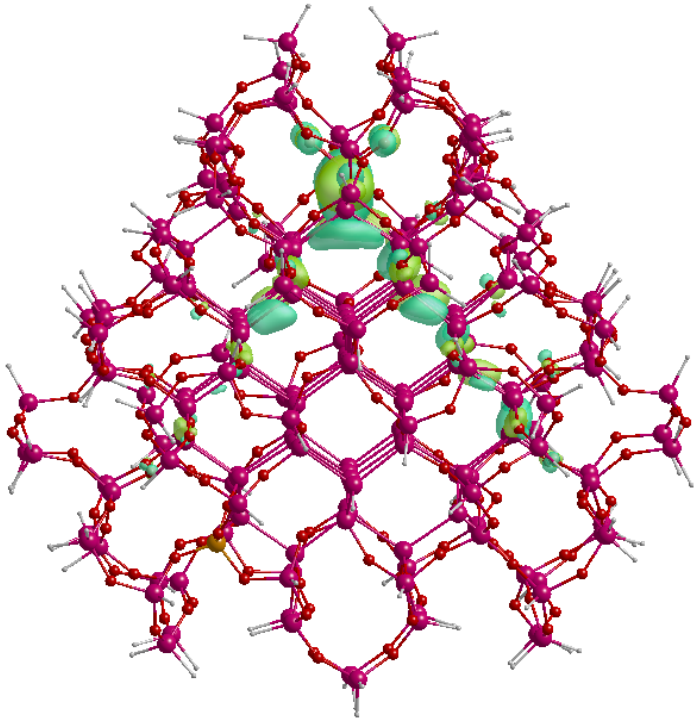

Figure 4.2: Isosurface plot of the HOMO level for the Si/SiO_2 crystal doped with P. 211 Si atoms (pink), 216 O atoms (red), 1 P atom (brown) passivated by 140 H atoms (white)

In order to calculate the absorption spectrum, one can appeal to a time-dependent DFT (TD-DFT) theory, that is implemented within Octopus. The absorption spectrum is evaluated by exciting the system with a very short pulse, and then propagating the time-dependent Kohn-Sham equations for a certain time. The spectrum is thus evaluated from the time-dependent dipole moment.

Bibliography

[1] J. Coutinho. *Oxygen-Related Point Defects in Silicon and Germanium.* PhD thesis, Universty of Exeter, 2002.

[2] M. P. Marder. *Condensed Matter Physics (chapter 9).* A Wiley-Interscience Publication, 2000.

[3] J. M. Thijssen. *Computational Physics.* Cambridge University Press, 1999.

[4] R. Jones and P. R. Briddon. *The Ab Initio Cluster Method and the Dynamics of Defects in Semiconductors*, chapter 6. Volume 51A, Semiconductors and Semimetals, Academic Press, Boston, 1998.

[5] W. Kohn and L. J. Sham. Self-consistent equations including exchange and correlation effects. *Physical Review*, 140:A1133–A1138, 1965.

[6] P. Hohenberg and W. Kohn. *Physical Review*, 136:B864, 1964.

[7] S. Kurth, M. A. L. Marques, and E. K. U. Gross. *Density Functional Theory*, chapter Encyclopedia of Condensed Matter Physics, pages 395–402. Elsevier, 2005.

[8] F. Nogueira, A. Castro, and M. A. L. Marques. *A Primer in Density Functional Theory*, chapter 6, pages 218–251. Springer, 2002.

[9] E. Fermi. *Il Nuovo Cimento*, 11:157, 1934.

[10] H. Hellmann. *Journal of Chemical Physics*, 3:61, 1935.

[11] R. M. Martin. *Electronic Structure - Basic Theory and Practical Methods.* Cambridge University Press, 2004.

[12] D. M. Ceperley and B. J. Alder. *Physical Review Letters*, 45:566, 1980.

[13] J. P. Perdew and A. Zunger. Self-interaction correction to density-functional approximations for many-electron systems. *Physical Review B*, 23:5048, 1981.

[14] J. P. Perdew and Y. Wang. Accurate and simple analytic representation of the electron-gas correlation energy. *Physical Review B*, 45:13244–13249, 1992.

[15] W. Koch and M. C. Holthausen. *A Chemist's Guide to Density Functional Theory*. Wiley-VCH Verlag GmbH, second edition edition, 2001.

[16] A. D. Becke. A new mixing of hartree-fock and local density-functional theories. *J. Chem. Phys.*, 98:1372–1377, 1993.

[17] J. P. Perdew and S. Kurth. *A Primer in Density Functional Theory*, chapter 1, pages 1–51. Springer, 2002.

[18] P. R. Briddon and R. Jones. Lda calculations using a basis of gaussian orbitals. *phys. stat. sol. (b)*, 217:131–171, 2000.

[19] R. Jones and J. Coutinho. *Germanium Based Technologies*, chapter 6, page 204. Elsevier Limited, 2007.

[20] L. E. Ramos, E. Degoli, G. Cantele, S. Ossicini, D. Ninno, J. Furthmüller, and F. Bechstedt. Optical absorpton spectra of doped and codoped si nanocrystallites. *Physical Review B*, 78:235310, 2008.

[21] F. Iori, E. Degoli, R. Magri, I. Marri, G. Cantele, D. Ninno, F. Trani, O. Pulci, and S. Ossicini. Engineering silicon nanocrystals: Theorectical study of the effect of codoping with boron and phosphorus. *Physical Review B*, 76:085302, 2007.

[22] F. Trani. *Electronic and Optical Properties of Silicon Nanocrystals: a Tight Binding Study*. PhD thesis, 2004.

[23] C. S. Garoufalis, A. D. Zdetsis, and S. Grimme. High level *Ab Initio* calculations of the optical gap of small silicon quantum dots. *Physical Review Letters*, 87:276402, 2001.

[24] S. Ögut, J. R. Chelikowsky, and S. G. Louie. Optical properties of silicon nanocrystals: A first principles study. In E. L. Shirley, J. R. Chelikowsky, S. G. Louie, and G. Mar-

tinez, editors, *The Optical Properties of Materials, MRS Symp. Proceed.*, volume 579, page 81. Materials Research Society, Warrendale, 2000.

[25] H. Ch. Weissker, J. Furthmüller, and F. Bechstedt. Structure- and spin-dependent excitation energies and lifetimes of si and ge nanocrystals form ab initio calculations. *Physical Review B*, 69:115310, 2004.

[26] S. Ögut and J. R. Chelikowsky. Quantum confinement and optical gaps in si nanocrystals. *Physical Review Letters*, 79:1770, 1997.

[27] L. X. Benedict, A. Puzder, A. J. Williamson, J. C. Grossman, G. Galli, and J. E. Klepeis. Calculation of optical absorption spectra of hydrogenated si clusters: Bethe salpeter equation versus time-dependent local-density approximation. *Physical Review B*, 68:085310, 2003.

[28] D. V. Melnikov and J. R. Chelikowsky. Electron affinities and ionization energies in si and ge nanocrystals. *Physical Review B*, 69:113305, 2004.

[29] I. Vasiliev, S. Ögt, and J. R. Chelikowsky. *Ab Initio* absorption spectra and optical gaps in nanocrystalline silicon. *Physical Review Letters*, 86:1813, 2001.

[30] E. L. de Oliveira, E. L. Albuquerque, J. S. de Sousa, and G. A. Farias. Radiative transitions in p- and b-doped silicon nanocrystals. *Applied Physics Letter*, 94:103114, 2009.

[31] A. Rockett, D. D. Johnson, S. V. Kahare, and B. R. Tuttle. Prediction of dopant ionization energies in silicon: The importance of strain. *Physical Review B*, 68:233208–233211, 2003.

[32] S. Ossicini, E. Degoli, F. Iori, O. Pulci, G. Cantele, R. Magri, O. Bisi, F. Trani, and D. Ninno. Doping in silicon nanocrystals. *Surface Science*, 601:2724–2719, 2007.

[33] P. Y. Yu and M. Cardona. *Fundamentals of Semiconductors*. Springer, Berlin, 2001.

[34] T.-L. Chan, M. L. Tiago, E. Kaxiras, and J. R. Chelikowsky. Size limits on doping phosphorus into silicon nanocrystals. *Nano Letters*, 8:596–600, 2008.

[35] T.-L. Chan and J. R. Chelikowsky. Controlling diffusion of lithium in silicon nanostructures. *NanoLetters*, 2010.

[36] D. V. Melnikov and J. R. Chelikowsky. Quantum confinemnt in phosphorus-doped silicon nanocrystals. *Physical Review Letters*, 92(4):046802–046805, 2004.

[37] R. N. Pereira, A. R. Stegner, T. Andlauer, K. Klein, H. Wiggers, M. S. Brandt, and M. Stutzmann. Dielectric screening versus quantum confinement of phosphorus donors in silicon nanocrystals investigated by magnetic resonance. *Physical Review B*, 79:161304, 2009.

[38] Z. Zhou, M. L. Steigerwald, R. A. Freisner, L. Brus, and M. S. Hybertsen. Structural and chemical trends in doped silicon nanocrystals: First-principles calculations. *Physical Review B*, 71:245308, 2005.

[39] C. Xia Yan, Y. Dai, and B. B. Huang. Dft study of halogen impurity in diamond. *Journal of Physics D: Applied Physics*, 42:145407–145412, 2009.

[40] S. A. Kajihara, A. Antonelli, and J. Bernholc. Nitrogen and potential n-type dopants in diamond. *Physical Review Letters*, 66:2010–2013, 1991.

[41] J. P. Goss and P. R. Briddon. Theorectical study of li and na as n-type dopants for diamond. *Physical Review B*, 75:075202, 2007.

[42] J. A. Weima, J. von Borany, K. Meusinger, J. Horstmann, and W. R. Fahrner. *Diamond Relat. Mater.*, 12:1307, 2003.

[43] R. Ruffo, S. S. Hong, C. K. Chan, R. A. Huggins, and Y. Cui. Impedance analysis of silicon nanowire lithium ion batery anodes. *J. Phys. Chem. C.*, 113:11390–11398, 2009.

[44] R. Jones and references therein. *Early Stages of Oxygen Precipitation in Silicon.* Kluwer Academic Publishers, Dordrecht, 1996.

[45] J. Coutinho, R. Jones, L. I. Murin, V. P. Markevich, J. L. Lindström, S. Öberg, and P. R. Briddon. Thermal double donors and quantum dots. *Physical Review Letters*, 87:235501, 2001.

[46] http://aimpro.ncl.ac.uk.

[47] http://www.tddft.org/programs/octopus.

[48] K. Sasaki and K. Wakabayashi. Chiral gauge theory for graphene edge. *arXiv:1003.5036v1[cond-mat.mes-hall]*, 2010.

[49] S. Goedecker, M. Teter, and J. Hutter. Separable dual-space gaussian pseudopotentials. *Physical Review B*, 54:1703–1710, 1996.

[50] C. Hartwigsen, S. Goedecker, and J. Hutter. Relativistic separable dual-space gaussian pseudopotentials from h to rn. *Physical Review B*, 58:3641–3662, 1998.

[51] Modified to improve the matching between the low and high rs parts.

[52] J. P. Perdew, K. Burke, and M. Ernzerhof. Generalized gradient approximation made simple. *Physical Review Letters*, 77:3865, 1996.

[53] J. P. Perdew, K. Burke, and M. Ernzerhof. Generalized gradient approximation made simple [phys. rev. lett. 77, 3865 (1996)]. *Physical Review Letters*, 78:1396(E), 1997.

[54] N. Troullier and J. L. Martins. Efficient pseudopotentials for plane-wave calculations. *Physical Review B*, 43:1993, 1991.

[55] E. Degoli, G. Cantele, E. Luppi, R. Magri, D. Ninno, O. Bisi, and S. Ossicini. *Ab Initio* structural and electronic properties of hydrogented silicon nanoclusters in the ground and excited state. *Physical Review B*, 69:155411, 2004.

[56] S. Ossicini, F. Iori, E. Degoli, E. Luppi, R. Magri, R. Poli, G. Cantele, F. Trani, and D. Ninno. Understanding doping in silicon nanostructures. *IEEE Journal of Selected Topics in Quantum Electronics*, 12(12):1585–1591, 2006.

[57] A. Pasquarello, M. S. Hybertsen, and R. Car. Interface structure between silicon and its oxide by first-principles molecular dynamics. *Nature*, 396:58, 1998.